Materials **2014**, *7*, 1687-1708; doi:10.3390/ma7031687

OPEN ACCESS

materials

ISSN 1996-1944

www.mdpi.com/journal/materials

Article

Osteoblasts Interaction with PLGA Membranes Functionalized with Titanium Film Nanolayer by PECVD. *In vitro* Assessment of Surface Influence on Cell Adhesion during Initial Cell to Material Interaction

Antonia Terriza [2], José I. Vilches-Pérez [1], Juan L. González-Caballero [1], Emilio de la Orden [1], Francisco Yubero [2], Angel Barranco [2], Agustín R. Gonzalez-Elipe [2], José Vilches [1] and Mercedes Salido [1,*]

[1] Facultad de Medicina, Universidad de Cádiz, Servicios Centrales de Investigación en Ciencias de la Salud, Dr. Marañon 3. 11002 Cádiz, Spain; E-Mails: drvilches@dentalcamposoto.es (J.I.V.-P.); juanluis.gonzalez@uca.es (J.L.G.-C.); emilio.delaorden@uca.es (E.O.); jose.vilches@uca.es (J.V.)

[2] Nanotechnology on Surfaces Laboratory, Instituto de Ciencia de Materiales de Sevilla (CSIC-Univ. Sevilla), Avda. Americo Vespucio 49, E-41092 Seville, Spain.; E-Mails: antonia.terriza@icmse.csic.es (A.T.); yubero@icmse.csic.es (F.Y.); angel.barranco@csic.es (A.B); arge@icmse.csic.es (A.R.G.-E.)

***** Author to whom correspondence should be addressed; E-Mail: mercedes.salido@uca.es; Tel.: +34-956-015-832; Fax: +34-956-015-265.

Received: 29 October 2013; in revised form: 10 February 2014 / Accepted: 25 February 2014 / Published: 4 March 2014

Abstract: New biomaterials for Guided Bone Regeneration (GBR), both resorbable and non-resorbable, are being developed to stimulate bone tissue formation. Thus, the *in vitro* study of cell behavior towards material surface properties turns a prerequisite to assess both biocompatibility and bioactivity of any material intended to be used for clinical purposes. For this purpose, we have developed *in vitro* studies on normal human osteoblasts (HOB®) HOB® osteoblasts grown on a resorbable Poly (lactide-co-glycolide) (PLGA) membrane foil functionalized by a very thin film (around 15 nm) of TiO_2 (*i.e.*, TiO_2/PLGA membranes), designed to be used as barrier membrane. To avoid any alteration of the membranes, the titanium films were deposited at room temperature in one step by plasma enhanced chemical vapour deposition. Characterization of the functionalized membranes proved that the thin titanium layer completely covers the PLGA foils that remains practically unmodified in their interior after the deposition process and stands the standard sterilization protocols. Both morphological changes and cytoskeletal

reorganization, together with the focal adhesion development observed in HOB osteoblasts, significantly related to TiO_2 treated PLGA in which the Ti deposition method described has revealed to be a valuable tool to increase bioactivity of PLGA membranes, by combining cell nanotopography cues with the incorporation of bioactive factors.

Keywords: adhesion; cell culture; osteoblasts; cell-material interaction; plasma enhanced chemical vapor deposition (PECVD); titanium; nanolayers; functionalization; PLGA; biomedical

1. Introduction

Bone insufficiency or defects arising from tumor, trauma, or periodontal diseases adversely affects the curative rates in oral medicine and orthopedy. Most concerning to clinicians is sufficient bone tissue, which is critical for successful therapy. Traditional methods including autografts, allografts, and xenografts usually have drawbacks, such as donor shortage, immunological rejection, or potential risk of disease transmission [1]. Despite many successful developments and improvements, implant dentistry still faces many challenges. Various risk factors that still exist, such as poor bone quality and quantity, systemic conditions, and smoking, may limit its application and decrease the success rate. Although various preimplant surgery are effective to expand implant applications, these surgical intervention increases patient morbidity, and clinical outcomes for these complex cases are not as predictable as those in regular placement cases. In light of this, increasing research for further improvement of dental implants properties in order to increase their ability and capacity of osseointegration is needed [2]. For clinical use, in addition to mechanical properties, surgical requirements, and ability to stand sterilization procedures, a biomaterial must interact adequately with the biological environment through its physical/chemical surface [3]. All of these shortcomings highlight the need for the development of better biomaterials for bone regeneration [1].

Biodegradable polymeric implants have become popular in the field of orthopaedics; however, there is only limited knowledge about the behavior of the surrounding osteoblast cells. Polylactide represents one class of biodegradable materials that have demonstrated both the biocompatibility and the capacity to support osteoblast-like cell growth *in vitro* [4]. As a synthetic polymer fabricated through copolymerization of glycolide and lactide, poly lactic-co-glycolic acid (PLGA) is widely used for bone tissue engineering and drug delivery due to its superior mechanical properties and controllable degradability. PLGA is known to be degraded by hydrolysis and is eliminated from the organism through the Krebs cycle as carbon dioxide and water. Therefore, it has been successfully used in biodegradable membranes for Guided Bone Regeneration (GBR). The strength of PLGA is equivalent to that of interosseous ligaments, but its hydrophobicity and relatively lower cell affinity than natural polymers limit its application [1].

To overcome such limitations, the surface modification of biomaterials aims to promote the osseointegration controlling the cells activities since the adhesion of osteoblastic cells can accelerate the bone apposition on the surface of the biomedical implants to constitute the interface [5].

The technologies for surface modification of synthetic polymers generally require complex reaction conditions and specific equipment, which greatly limit the application and result in unreliable effects. Thus, a simple but effective method for surface modification of PLGA is required [1]. For several years, tissue engineers have focused on improving the performance of polymers, such as poly-L-lactide acid (PLLA) and polylactide-co-glycolic acid (PLGA) by introducing functional groups onto the polymer or by modifying their morphology or surface topography [4].

Titanium (Ti) and its alloys are used extensively for medical devices in dental, orthopaedic, and cardiovascular fields due to their superior mechanical property, relatively low elastic modulus, high corrosion resistance and excellent biocompatibility, with the capacity to interact with bones and other tissue without any cytotoxic effects [6,7]. We have previously described, on UV illuminated amorphous TiO_2, a positive effect on osteoblasts development that can be attributed to the transformations undergone by the surface of the oxide subjected to irradiation [8].

Nevertheless, although surface topography of titanium implants has been shown to modulate the percentage of bone-implant contact and the mechanical strength of bone-implant attachment [9,10], titanium and its alloys are bioinert materials. Indeed, titanium implants do not chemically bond to the bone [11,12].

In vitro analyses have shown that topography, composition, roughness, and surface energy are important factors to a biological performance [5,7]. Furthermore, the *in vitro* study of cell behavior toward different material surface properties represents a necessary prerequisite in assessing the biocompatibility of a material intended to be used in medical devices [3]. Tissue engineering offers a promising solution for development of synthetic and/or natural scaffolds, upon which osteoprogenitor cells can be seeded and cultured under optimal conditions and, ultimately, implanted to promote osteogenesis *in vivo* [8]. Though recent studies report decisive positive effects on cells, they frequently employ cells other than of human origin or cells not representing oral implant targets.

As is well known, cell internal organization and orientation are controlled by focal adhesions, that mediate the regulatory effects of extracellular matrix ECM adhesion and the variation of actin- myosin stress fibers distribution in response to surface properties [13,14] and, as we have previously described, associates with an substantial increase in osteoblastic mitocondrial bioenergetics polarized to focal adhesion sites [8,14]. Focal adhesions FAs are formed during initial cell adhesion and thereafter constantly assembled and disassembled during cell movement. These integrin-based FAs serve as mechanosensors converting environmental mechanical cues into biological signals [15,16].

In this study, we have investigated a novel methodology for tailoring the surface of biodegradable PLGA membranes by functionalization with a TiO_2 layer prepared by plasma enhanced chemical vapor deposition (PECVD) [17]. This is a dry method of deposition that preserves the integrity of the PLGA membranes and permits an accurate control over the TiO_2 thickness. Over other wet chemical routes, this method presents the advantage of working at room temperature, the possibility of being carried out in one step and that it does not produce significant amounts of waste substances. The main goal is the analysis of human osteoblasts adhesion and behavior on these nano TiO_2/PLGA tailored membranes by assessing the influence of the amount of deposited TiO_2 on their bioactivity. For this purpose three types of membranes have been synthethized with increasing nominal thickness of TiO_2 from 10 to 100 nm. An important aspect of this work has been the assessment of the coverage degree of the PLGA substrate with the oxide, in particular the ascertainement of whether the surface is

completely covered by TiO_2 or if this material completely covers the polymeric substrate. For assessing this point we have used the X-ray photoemission spectroscopy (XPS), in an unconventional way, consisting of analyzing the shapes of the background of the spectra behind the elastic photoemission peaks [18]. The membranes were characterized, and the effects on cell proliferation and behavior including cytotaxis, adhesion, and migration were investigated.

2. Results and Discussion

2.1. Results

2.1.1. Analysis of the TiO_2 Distribution on the PLGA Substrate

Analysis of the surface of the TiO_2 modified PLGA substrates by atomic force microcopic only showed a slight increase in roughness after the plasma deposition of the oxide (*i.e.*, from 0.34 nm for the bare PLGA to typical values between 0.4 and 0.5 nm for the TiO_2 covered PLGA membranes). No distinction from patches of TiO_2 or free zones of PLGA could either be made with this technique. Therefore, to get some suitable information about the surface topology of the TiO_2/PLGA membranes, we propose the use of the XPS technique in a non-conventional manner: by studying the background behind the elastic peak signals.

The TiO_2 layers deposited by PECVD under the conditions described in the experimental section were amorphous, as confirmed by XRD. The XPS Ti2p spectrum in the TiO_2/PLGA samples is characterized by a Ti2p3/2 BE of 458.4 eV, typical of the Ti^{4+} oxidation state of this element, proving that titanium is deposited in the form of TiO_2. Meanwhile, the O1s spectrum of the investigated samples was characterized by a first peak at 529.8 eV due to the oxygen ions of TiO_2 convoluted with a braod shoulder at approximately 532.5 eV due to the different oxygen groups of this polymeric mixture. The C1s spectrum of the bare PLGA consisted of well defined three bands at 284.6, 287.5, and 288.5 eV attributed to C–C/C–H, COO, and COR functional groups in these composite polymer. In the TiO_2/PLGA samples, this spectrum appears distorded by a progressive decrease of the band intensities due to the polymer functional groups of PLGA. For sample TiO_2/PLGA-100 the spectrum was dominated by a small single band at 284.6 eV due to adventitious carbon deposited on the surface of TiO_2 overlayer. The atomic percentages determined from the area of the C1s, O1s and Ti2p photoemission peaks and the corresponding sensitivity factor of these elements (Table 1) reveal a continuous increase in the titanium concentration with the nominal thickness of deposited TiO_2. At the end, for sample TiO_2/PLGA-100, the data in Table 1 suggest the complete coverage of the PLGA substrate and that the remaining carbon is due to adventitious contamination.

An important clue for the present investigation was to ascertain whether the TiO_2 was completely covering the PLGA substrate, particularly for the lower nominal thicknesses of the oxide. Figure 1 shows a series of normalized wide scan spectra around the C1s peak corresponding to samples PLGA, TiO_2/PLGA-10, PLGA-30, and TiO_2/PLGA-100. It is apparent in this figure that the background behind the photoemission peak increases in intensity with the nominal thickness of deposited TiO_2. The spectra have been analized with the QUASES software [19] under the assumption that TiO_2 is deposited on the surface of the PLGA (*i.e.*, it does not penetrate within the polymer). The analysis provides information about the formation of patches of this oxide on the surface of the polymer. The

basic principle of the method relies on describing properly the inelastic losses induced by electron transport through a given material. It is assumed that, after excitation by the X-rays, the primary spectrum $F(E)$ transforms into the actually measured spectrum $J(E)$ (*i.e.*, Figure 1a) because of the energy losses undergone by the primary electrons during their transport through the analyzed material. For the analysis carried out here, it is assumed that the $F(E)$ function for carbon in PLGA corresponds to a homogeneous in-depth distribution of this element and that the probability for energy losses due to electron transport is governed by the polymer-type inelastic scattering cross sections included in the QUASES software package [19]. After applying this software to the experimental $J(E)$ spectra, one obtains the primary spectra in Figure 1b, where we report the results for sample TiO_2/PLGA-10.

Table 1. Atomic composition in percentages determined from the elastic peak areas, and island thickness and coverage degree determined from the QUASES analysis of the different TiO_2/PLGA samples.

Sample	Atomic composition			TiO_2 distribution (QUASES analysis)	
	%O	%Ti	%C	Island height (nm)	Surface coverage degree (%)
PLGA	46	–	54	–	0
TiO_2/PLGA-10	56	14	30	11	55
TiO_2/PLGA-30	57	15	28	26	60
TiO_2/PLGA-100	62	25	13	100	100

Figure 1. QUASES analysis of the TiO_2/PLGA samples. (**a**) C1s spectra of the indicated samples reporting a large background behind the elastic photoelectron peak; (**b**) comparison of the calculated and background subtracted spectra of sample TiO_2/PLGA-10 using the QUASES software and model of TiO_2 patches deposited on PLGA (inserted figure) [19].

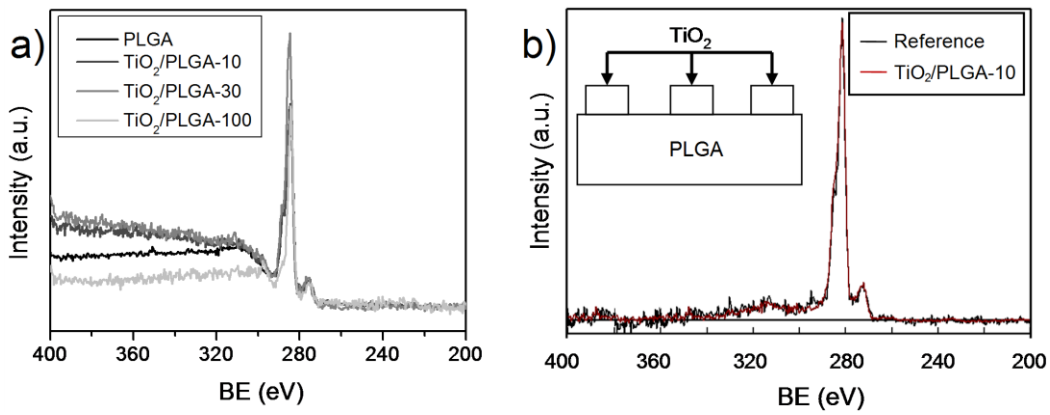

The good concordance between the calculated and background substrated spectra confirm the reliability of the analysis and that the determined distributions of TiO_2 as deposited patches on the surface of the PLGA is a good description of the surface state. Table 1 gathers the main morphological parameters of these samples, namely the approximate coverage degree of the PLGA substrate and the height of the TiO_2 partches taken as rectangular (see the enclosed scheme in this figure). This means that in samples TiO_2/PLGA-10 and TiO2/PLGA-30 the substrate is only partially covered by TiO_2 and that the osteoblast cells will experience both the effect of the PLGA and that of the TiO_2. In sample

TiO_2/PLGA-100, titanium oxide is completely covering the substrate and, therefore, the observed carbon signal should be attributed to adventitious carbon adsorbed on top of the oxide layer.

2.1.2. Cell Morphology and Spreading

Attachment, cell growth and phenotypic changes of osteoblasts grown *in vitro* appeared to be substantially better in cells grown on TiO_2 nanolayered PLGA than in cells grown on the bare substrata. Furthermore, living osteoblasts examination 24 h from seeding revealed a successful cell attachment with marked phenotypical changes, like filopodial and lamellopodial emission, and an improved cell spreading related to the nanolayer thickness (Figure 2). In this figure it is also apparent the formation of a series of lines attributed to the different agglomeration of the active phase during the preparation of the membrane. In relation with this behavior and in line with a previous work of our group on the osteoblast growth on PET surface modified with TiO_2 [8], it is worh noting that after UV illumination for sterilization, the TiO_2/PLGA membranes became superhidrophilic. It is believed that this enhanced hydrophilicty plays a very poisitve role in enhancing the deployment of osteoblast on these modified surfaces.

Figure 2. HOB cells spreading after 24 h in culture. (**A**) Osteoblasts grown on bare PLGA. Osteoblasts grown on TiO_2 functionalized PLGA membranes are shown correlatively in (**B**,**C**,**D**) after seeding on TiO_2/PLGA-10, TiO_2/PLGA-30, TiO_2/PLGA-100. Arrows for filopodial emissions. All images were obtained in a DM ILLED Leica inverted microscope, DIC mode, (A,C,D) magnification 20×; (B) magnification 40×.

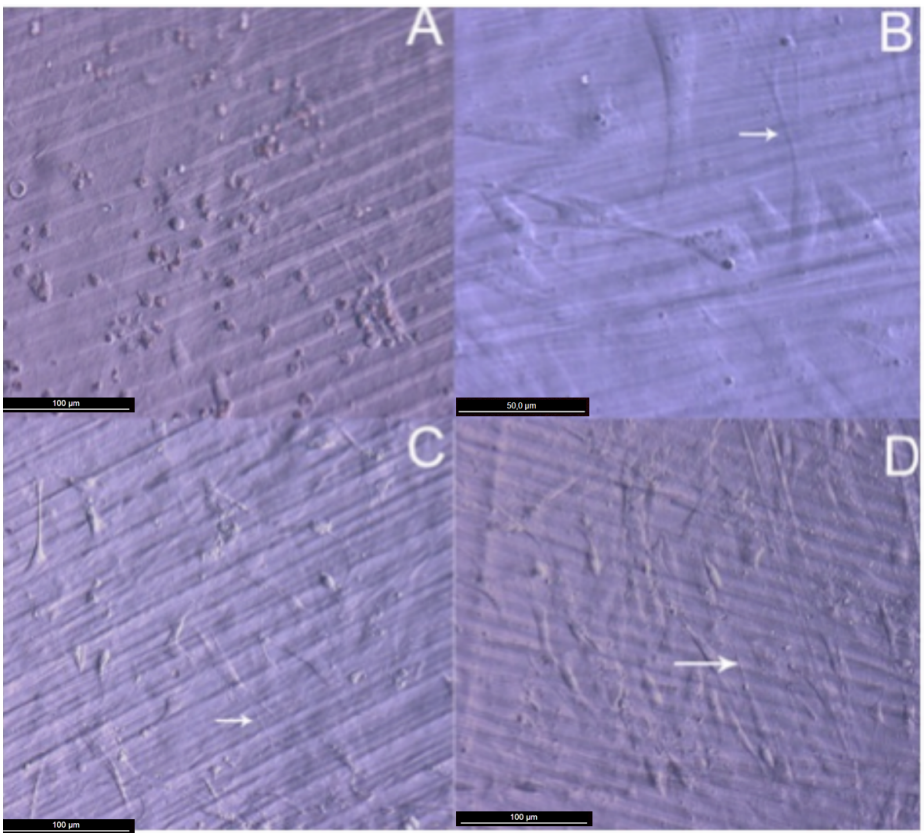

After 48 h in culture, the differences in cell spreading between osteoblasts grown on bare or TiO_2 nanolayered PLGA became much more evident, showing in the latter how cell spreading had evolved to a near confluence stage, with well differentiated osteoblasts adhered to the surface and tethering contacts to the neighboring cells. It is also apparent that TiO_2/PLGA-100 samples, where the complete substrate is covered by TiO_2, appeared to be more efficient in inducing cell spreading to confluence on functionalized surfaces. Osteoblasts grown on bare PLGA, although well adhered, did not spread to confluence, showing discrete cell overlapping after 48 h in culture (Figure 3).

Figure 3. HOB cells spreading after 48 h in culture. (**A**,**B**) Osteoblasts grown on bare PLGA. Osteoblasts grown on TiO_2/PLGA-10 are shown in (**C**,**D**); TiO_2/PLGA-30 in (**E**,**F**); and TiO2/PLGA-100 (**G**,**H**). Arrows for filopodial emissions .All images were obtained in a DMILLED Leica inverted microscope, DIC mode, (A,C,E,G) magnification 20×; (B,D,F,H) magnification 40×. Scale bar = 100 μm (A,C,E,G); Scale bar = 50 μm (B,D,F,H).

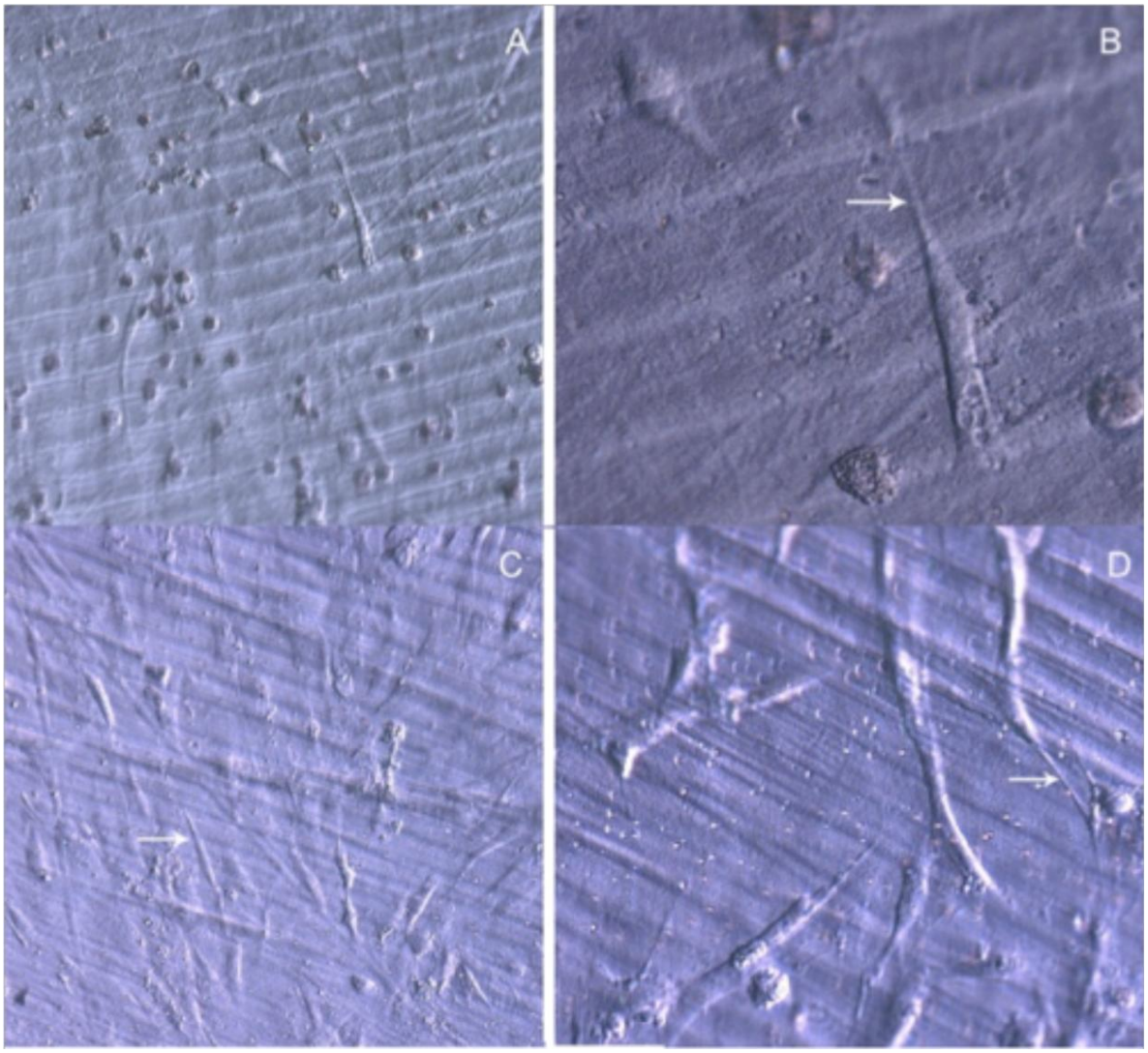

Figure 3. *Cont.*

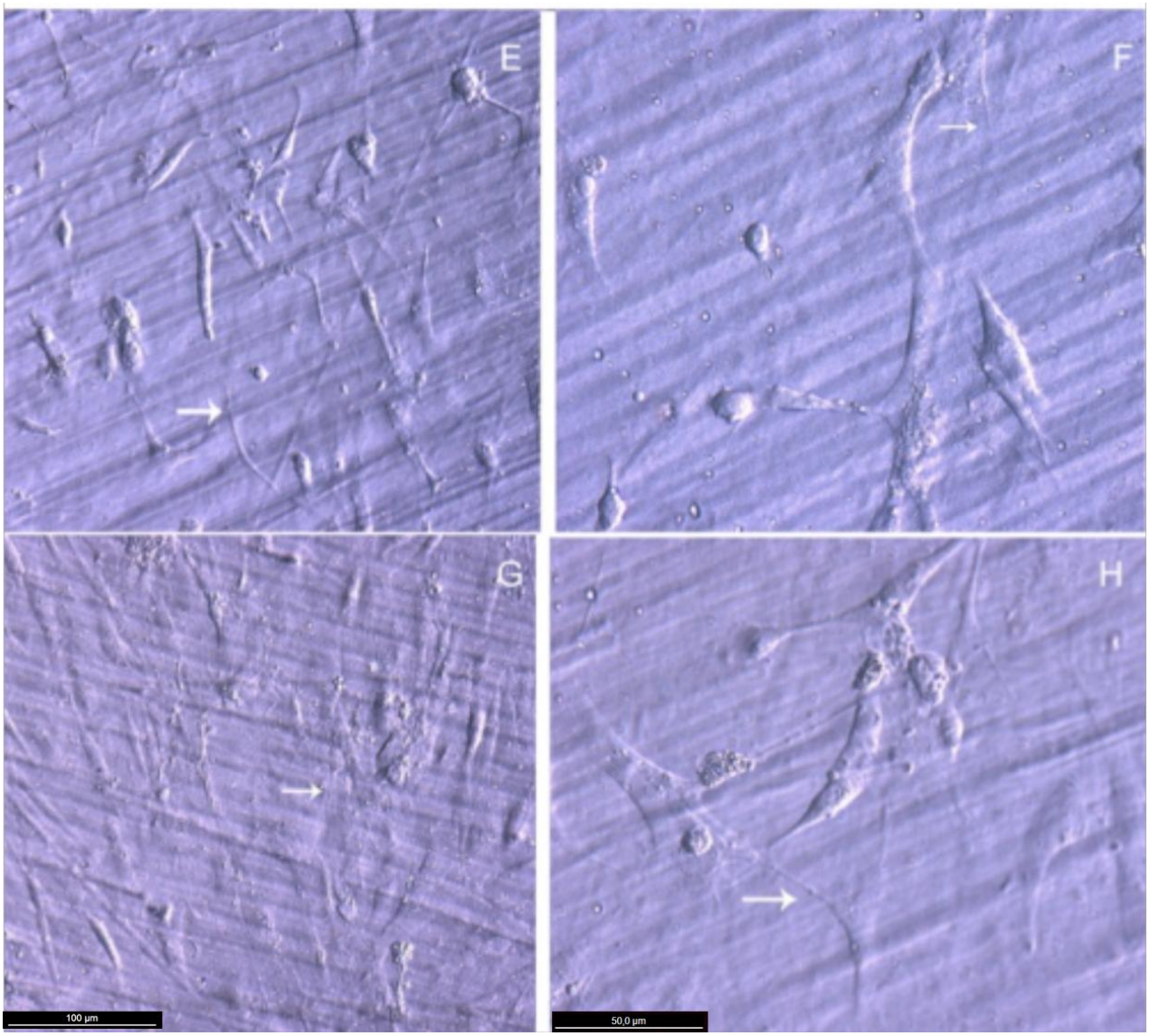

2.1.3. Cytoskeletal Organization and Focal Adhesions

Actin cytoskeleton immunolabelling of growing cells revealed clear differences both in cell behavior and in cytoskeletal arrangement. Osteoblasts grown on TiO_2 nanolayered PLGA were phenotypically elongated and clustered in a reticular pattern from 48 h in culture onwards, mostly in the TiO_2/PLGA-30 membranes (Figure 4). When the thickness of the nanolayer increases, osteoblasts elongated and in the TiO_2/PLGA-100 membranes, a higher polarization and stress fibers development, and a more defined osteoblast orientation was found, together with a higher number of well-developed focal adhesions. Cells grown on both TiO_2/PLGA-10 and TiO_2/PLGA-30 membranes showed a higher number of well developed focal adhesions (Figure 5) than in those grown on bare PLGA, mainly evident after 72 h in culture (Figure 6).

Figure 4. HOB cells grown on TiO_2 functionalized membranes, and imunolabelled with rhodamine-phalloidine for actin cytoskeleton 48 hours after seeding. Representative images of cytoskeletal features, showing in detail the differences in stress fibers development, cell clustering, lamellopodial and filopodial emissions. (**A**,**B**) Osteoblasts grown on TiO_2/PLGA-10, magnification 20× (**C**,**D**) TiO_2/PLGA-30, magnification (**C**) 20× and (**D**) 40×; (**E**,**F**) TiO_2/PLGA-100, magnification 20×.

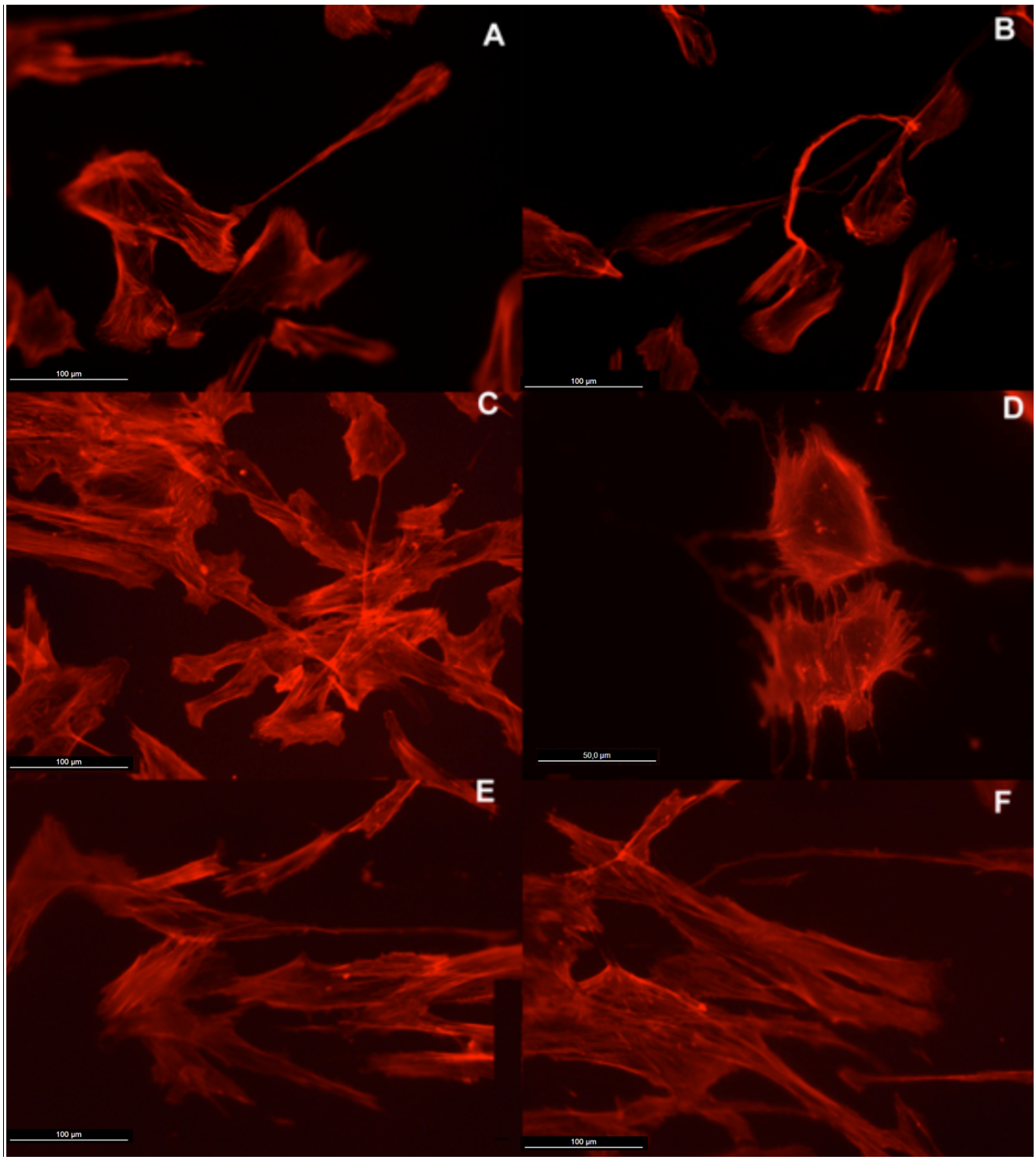

Figure 5. HOB cells grown on TiO_2 functionalized membranes, and imunolabeled with rhodamine-phalloidine for actin cytoskeleton (red) and antivinculin antibody (green) for focal adhesion sites, 72 h after seeding. Representative images of cytoskeletal features, showing the differences in stress fibers, and focal adhesion sites vinculin-dependent. Osteoblasts grown on (**A**,**B**,**C**) TiO_2/PLGA-10; (**D**,**E**,**F**) TiO_2/PLGA-30; (**G**,**H**,**I**) TiO_2/PLGA-100. Combined, overlay, images for both rhodamine-phalloidine labeling and antivinculin antibody for each group are shown in (**A**,**D**,**G**). Magnification 40×. Scale bar = 50 μm.

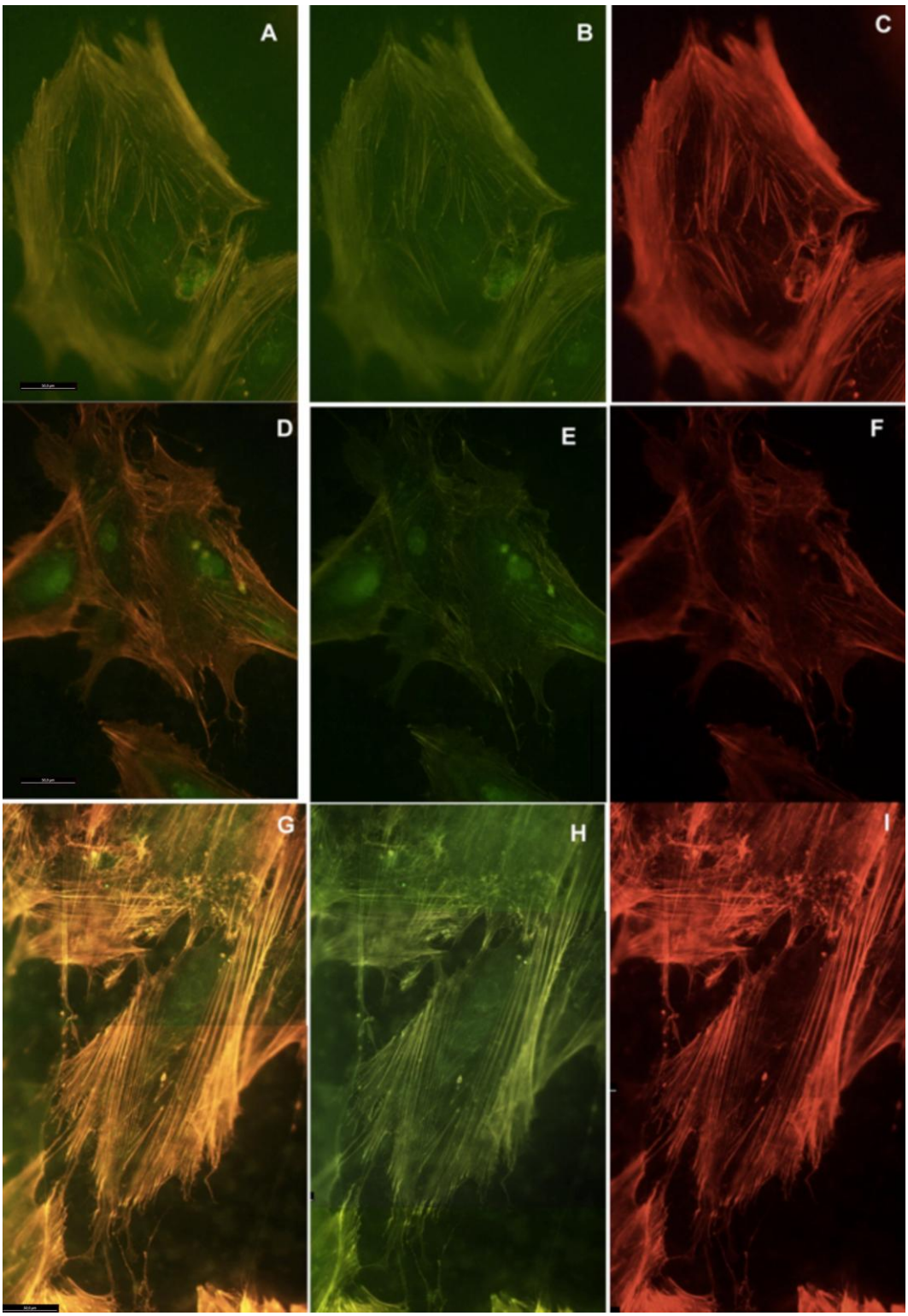

Figure 6. HOB cells grown on bare PLGA and imunolabeled, (**A,C**) 48 h and (**B,D**) 72 h after seeding, with rhodamine-phalloidine for actin cytoskeleton (red) and antivinculin antibody (green) for focal adhesion sites. Magnification 40×. Scale bar = 50 μm.

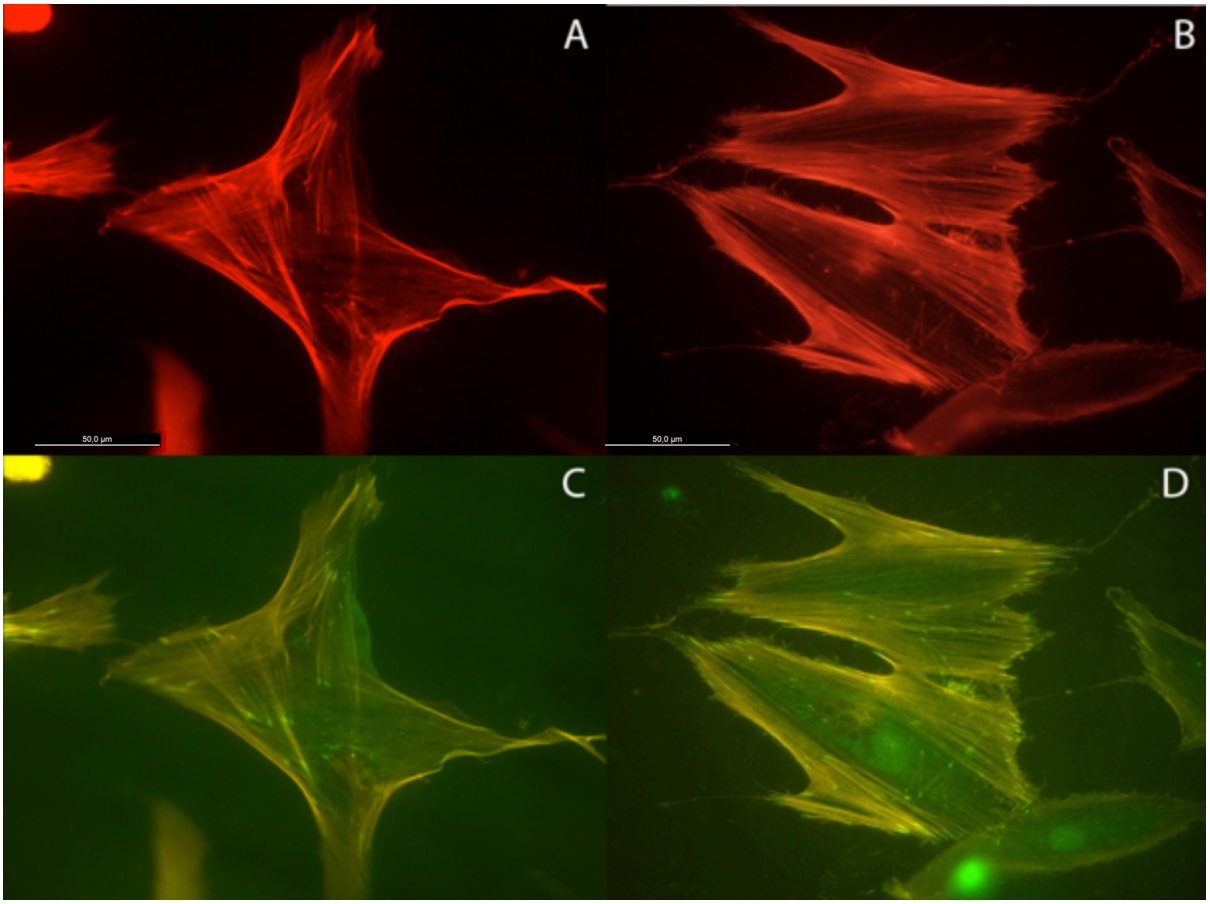

2.1.4. Statistical Analysis

An analysis of the common descriptives parameters (Table 2) and the Box- Whisker graphic (Figure 7) performed on the focal adhesions detected in the different groups revealed that, even tough after 48 h in culture no significant difference in the development of focal adhesions was found when osteoblasts were grown in any test surface, whenever they were covered or not by the TiO_2 nanolayer, when osteoblasts were kept in contact with the tested surfaces for 72 h, clear differences in focal adhesions development were found between the TiO_2/PLGA-30 and TiO_2/PLGA-100 functionalized groups and the control group, bare PLGA, or the the TiO_2/PLGA-10 group. After the descriptive analysis, the non-parametric K-W test was performed in order to confirm the role of TiO_2 nanolayers in the development of focal adhesions obtained, obtaining an statistic H = 27.274 that provides a high significance ($p = 0.000$; $gl = 7$) and indicates a clear effect, which can be attributed to the TiO_2 nanolayers, time, or both.

Table 2. Descriptive data per group.

	Groups	% Area	Contacts per group				
			Mean	SD	Median	Min	Max
1	PLGA Clean 48 h	7.75	134.29	35.59	139.00	96	191
2	PLGA+TiO_2 10 nm 48 h	24.62	133.82	32.08	130.00	87	189
3	PLGA+TiO_2 30 nm 48 h	31.34	128.00	37.28	118.00	94	192
4	PLGA+TiO_2 100 nm 48 h	33.57	130.00	21,20	130.00	105	155
5	PLGA Clean 72 h	9.02	81.86	51,51	69.00	28	159
6	PLGA+TiO_2 10 nm 72 h	21.75	99.75	72,08	80.50	42	196
7	PLGA+TiO_2 30 nm 72 h	27.31	169.5	44,30	172.50	101	245
8	PLGA+TiO_2 100 nm 72 h	32.52	218.57	31. 90	208.00	188	272
	Total	–	145.06	54.15	137.00	28	272

Figure 7. Box-Whisker graphics reporting the variable number of contacts detected on cells grown on each studied sample.

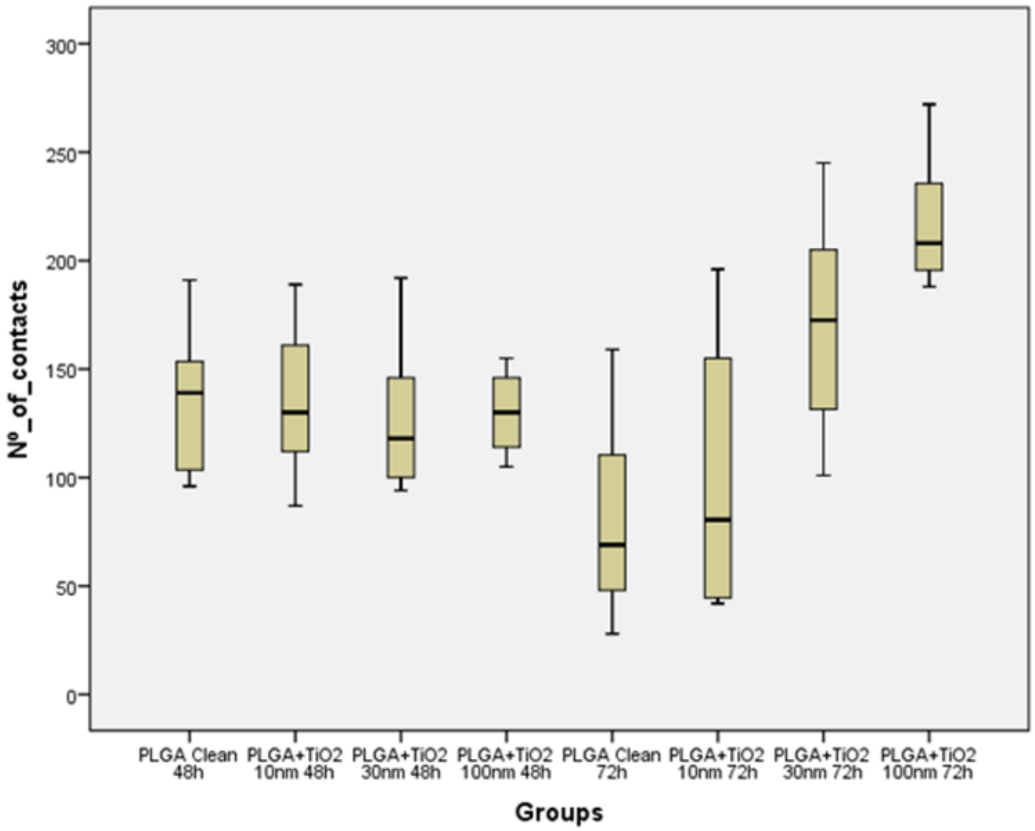

In order to take advantage of the experimental design [20], a parametric two-way ANOVA on ranks of the variable was performed, with factors TiO_2 and time, to compare the effect of each factor separately, and their interaction on the variable "ranks of focal adhesions". The results of this analysis indicate that the model is able to explain 41.3% of the variability of ranks of focal adhesions, the TiO_2 is a significant factor ($p = 0.000$) while the time factor is not significant ($p = 0.18$)) and is also significant the interaction between the two factors ($p = 0.001$). These results indicate that the groups defined by different amounts of titanium oxide (clean, 10, 30, 100 nm TiO_2) present differences in the number of contacts, while it cannot say the same with respect to the groups defined by the time factor

(48 and 72 h). Moreover, the interaction indicates that different amounts of titanium oxide did not remain homogeneous between 48 and 72 h, as plotted in figure (Figure 8).

Finally, the *post hoc* contrast S-N-K on the 8 treatment groups (Table 2), clearly indicates the existence of three distinct partnerships of treatments ($p < 0.05$). The first partnership contains groups 5 and 6, the second group contains 1, 2, 3, 4 and 7, and the third contains the group 8.

Figure 8. Interaction on the variable "ranks of focal adhesions" of factors TiO_2 and time.

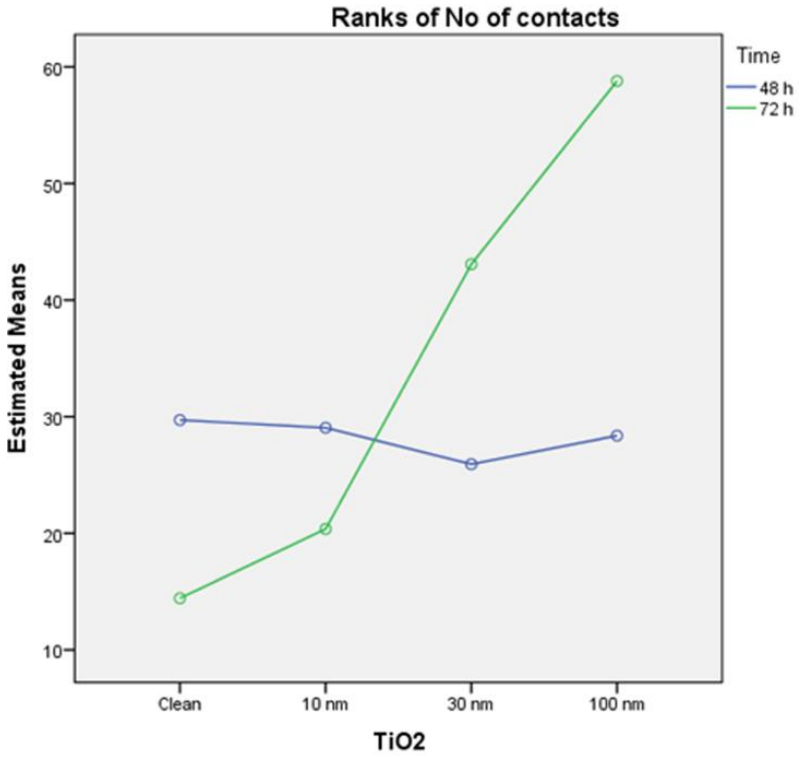

2.2. Discussion

With the advent of nanotechnology, there has been an interest in using this emerging science for various orthopaedic applications and considerable research has been devoted to modification of titanium oxide surfaces by coating, chemical modification, and nanostructuring to provide the metal oxide with bone-bonding ability and thus improve dental implant osseointegration. In this sense, PLGA is a polymeric biocompatible material which degrades into non-toxic products that do not adversely affect cell metabolism and has been proven to increase osseointegration, decrease fibroblast growth, and help stabilize implants [21–23].

To take advantage of these properties, we, herein, propose an alternative method to improve bone guided regeneration, with the novel design of a barrier composite membrane of PLGA functionalized by PECVD with titanium oxide nanolayers. The function of this membrane would be two-fold. First to serve as isolation barrier to prevent the colonization by cells other than osteoblasts, and second to favor the deployment of these latters on the TiO_2 bioactive surface, particularly after their UV illumination [8]. In addition, after some weeks these membranes (50 micron thick) would be resorbable by the body practically not leaving any trace of residues (note the very tiny size of the TiO_2 patches or layers covering the PLGA).

The process of cell adhesion on materials depends on various parameters incluiding topography, chemistry, or composition of the material. The term ‘adhesion’ in the biomaterial domain covers different phenomena. It is a step-by-step process from the initial contact to a long-term cell response.

Cell migration requires a dynamic interaction between cell, substrate, and cytoskeleton. As shown in our data, first, cells develop a protrusion of their leading edge to form a lamellipodium. Second, after lamellipodium formation and fixation, cells use adhesive interactions to generate the traction and energy required for cell movement [24–26]. The last step of the migratory cycle is the release of adhesions at the rear part of the cell followed by its detachment and retraction. During cell spreading and locomotion the assembly of early cell contacts to the ECM at the leading edge are driven by actin polymerization. In the nearby lamella, actomyosin contraction plays a major role in regulating FA structure and dynamics as well as the position of the cell’s front consequently affecting the progression of the spreading or migration process. Thus, the focal adhesions that are formed during spreading serve as cytoskeletal organizing centers as well as surface-sensing entities that control, locally and globally, adhesion-mediated signaling and coordinate the adhesive and migratory process. When the attachment and initial behavior of osteoblasts were examined in our model, Magnified confocal images revealed that cells on functionalized surfaces were more elongated than those on untreated surface from the initial 24 h. Cytoplasmic pro jections, such as filopodia and lamellipodia, had already developed in most cells on functionalized surfaces at this early time point and cell tethering appears more evident in the composite membranes in which the Ti nanolayer is is in the form of patches, *i.e.*, samples TiO_2/PLGA-10 and TiO_2/PLGA-30, at 24 or 48 h experimental times, while osteoblasts grown on sample TiO_2/PLGA-100, with the TiO_2 covering completely the PLGA substrate, appeared to be clearly settled in at the same experimental times. These data are reinforced when vinculine-based focal adhesion sites were analyzed, showing significant differences at 72 h between composite groups and bare PLGA membranes.

Following activation and ligand binding, integrins cluster together into nanoscale adhesive structures that function as foci for the generation of strong anchorage and traction forces in stationary and migrating cells [16,27].

Traction forces, generated by the actin-myosin II cytoskeleton, are transmitted to the extracellular matrix through the associated focal adhesion complexes. Active traction forces are concentrated at the frontal periphery and are oriented toward the cell center, consistent with a propulsive role during cell migration: (1) initially, the cell forms small focal adhesions as it adheres to the substrate; (2) these small focal adhesions produce weak traction stresses, which allow the cell to start probing mechanical properties of the substrate; (3) positive feedback from the initial probing forces serves to stimulate the assembly of the actin cyto-skeleton, which in turn stimulates further spreading, formation of larger focal adhesions, and generation of stronger forces and (4) this positive cycle continues, leading to a continuous increase in the size of focal adhesions and magnitude of traction stress until the cell reaches its limit of spreading or fills up the adhesive area [28].

The images presented show that the osteoblasts are well spread and attached to each of the surfaces, indicating that polymer coatings–were able to support osteoblast attachment and viability. Moreover, actin cytoskeletal development within the cytoplasm, as clearly stained by rhodamine, revealed that on bare PLGA most adhesive cells reach an extended polygonal shape and form large cables of actin filaments, in the proximity of cell membrane, rhodamine-positive, similar to cells allowed to adhere

and spread without constraints, and in HOB migrating cells, grown on the TiO_2/PLGA-10 and TiO_2/PLGA-30 samples on the 10 nm or 30 nm nanolayered PLGA, actin filaments are primarily organized into submembrane meshworks that appear diffuse or in small bundles, whereas stationary cells, mainly found on the on the TiO_2/PLGA-100 nm samples, usually display conspicuous arrays of filament bundles, "stress fibers", which are anchored at their termini in the matrix attachments known as focal adhesions. Furthermore, vinculin, was expressed in the extensive area of the cells on functionalized surfaces, with a particular positivity at the tips of cytoplasmic projections. The differences in these initial attachment and spreading behaviors were mostly evident after 72 h of incubation, and related to nanolayer thickness. In contrast, the cell membrane was rarely stained with vinculin in cells on untreated surface, in accordance with some authors that propose a dependence of traction stress on center-periphery distance represents an economic strategy for cells to conserve energy during spreading [1,2,29–33].

Previously, quantification of adhesions in osteoblasts in response to osteogenic nanotopographies showed that a reduction in the number of adhesions, but maintenance of the elongate adhesion size, was important for phenotypic progression [34,35]. Our finding that vinculin is involved in the reorganization of the cortical cytoskeleton in response to Ti nanofunctionalized PLGA surfaces suggests, in accordance with others, that this protein is more than just a simple linker or adaptor molecule that couples components of the cadherin and integrin family of cell adhesion molecules to the actin filament network [36–39]. From our data, it is conceivable that vinculin functions to coordinate cell migration by stabilizing cell–cell and cell–matrix contacts of stimulated cells in an adequate microenvironment.

In summary, the analysis of focal adhesions and human osteoblasts presented in our model demonstrates that there are distinctions between HOB cells cultured on bare PLGA and nanofunctionalized Ti substrata during early, "decision-making", stages of osteoblasts commitment with a significant relationship between nanolayer thickness and cell response. Osteoblasts grown on the thicker nanolayer where TiO_2 completely covers the PLGA substrate (*i.e.*, TiO_2/PLGA-100 sample) expressed, in a time dependent way, a higher number of efficient focal adhesion sites, vinculin dependent, together with a higher stress fibers development. Our results demonstrate that the nanolayer deposited by PECVD creates a tailored PLGA scaffold in which the titanium oxide nanolayer plays a similar role to the one we have previously described , both for metallic titanium (likely covered with a natural TiO_2 thin layer formed by air exposure) and for nanolayered TiO_2 deposited on non resorbable polymers [8], thus, modulating focal adhesion and vinculin pathways.

3. Experimental Section

3.1. PLGA Membranes

The PLGA membranes used as substrates were prepared from a 1.5 wt% PLGA dichloromethane solution by evaporation of the solvent on a teflon plate. The thickness of the membrane foils was of the order of 50 microns. This small thickness ensures that these membranes inserted *in vivo* would be naturally degraded after a few weeks.

3.2. Deposition and Characterization of TiO_2 Thin Film Layers

TiO_2 was deposited at room temperature on the PLGA membranes by PECVD in a remote configuration reactor described in detail in previous works [27]. The system consisted of an external microwave plasma source (SLAN, Plasma Consult, GMbh, Germany) separated from the reactor chamber by a grounded grid to avoid the microwave heating of the PLGA substrates. Distance from substrate and grid was 10 cm. The system was operated at 400 W with pure O_2 as plasma gas. Titanium tetrakis isopropoxide (TTIP) was used as titanium precursor. The TTIP was placed in a stainless steel receptacle through which oxygen was bubbled while heating at 305 K. The precursor dispenser in the chamber and the dosing line were heated at 373 K to prevent condensation in the tube walls. Total pressure during deposition was 4×10^{-3} Torr. The amount of deposited TiO_2 was controlled by a quartz crystal monitor (QCM) placed close to the substrate that was calibrated by comparison with the scanning electron microscope cross section images of thick films deposited on a flat silicon substrate. In the course of this calibration analysis it was realized that the nominal thickness determined with the QCM was higher than the actual thickness determined by SEM. Nevertheless, for convenience, the samples will be referred to the nominal thickness directly determined during the deposition process with the QCM. To avoid any damage of the PLGA substrate by the plasma, before deposition of the titanium dioxide the substrate was protected with a shutter until stabilization of the plasma discharge in the presence of the precursor. Thin layers of TiO_2 with nominal thickness of 10, 30 and 100 nm as determined with the QCM were deposited on the polymeric substrate. These samples will be designated as TiO_2/PLGA-10, TiO_2/PLGA-30, and TiO_2/PLGA-100. They were characterized by XPS to determine the surface chemical state and composition, as well as the distribution of the oxide on the polymeric substrate. This latter analysis aims at ascertaining whether the TiO_2 forms a continuous film on the PLGA substrate or it is agglomerated in the form of islands on its surface. In this case the surface in contact with the biological medium would consist of patches of free PLGA and TiO_2 islands. For nanometric features of TiO_2 deposited on a polymer surface this analysis is not straightforward by direct microscopy observation (e.g., by AFM, possible changes in roughness could be associated to some preferential etching of the polymeric substrate during the initial deposition stages). Therefore, in the present work we have employed the XPS peak shape analysis developed by Tougaard [28,40]. This analysis provides a semiquantitative description of the island distribution of a material supported on a substrate, even if this latter presents a certain roughness. It has been previously used to ascertain the distribution of supported oxides or metals on inorganic substrates [18,41,42] or of atomic species within polymers [43] but, to our knowledge, not for polymers as substrates. This analysis requires a careful acquisition of the photoelectron spectra, not only around the elastic photoemission features but also of the backgrounds extending several tenths of electron volts behind the elastic peaks. The QUASES software of XPS peak shape analysis [19] was used to determine the PLGA surface coverage and TiO_2 islands height. This method relies on the fact that the inelastic background that appears in the low kinetic energy side of a photoelectron peak carries information on the distribution on the surface and/or in-depth of the atomic species of origin of the detected electrons [18,19,28,40–43]. Wide scan spectra of C1s, O1s and Ti2p peaks (*i.e.*, including their inelastic background) were analyzed according to this procedure. The analysis has been carried for the C1s peak because the relatively close binding energies (BEs) of the Ti2p and O1s peaks and the

contribution from both the PLGA substrate and the TiO_2 overlayer to this latter peak hamper the implementation of this methodology of analysis in these two cases.

XPS spectra were recorded with a SPECS XRC 1000 spectrometer working in the constant pass energy mode fixed at a value of 20 eV. The MgKα radiation was used as excitation source. For calibration of the BE scale, a value of 284.6 eV was considered for the C1s component attributed to C–H and C–C bonds.

3.3. Cell Culture

HOB® human osteoblasts (Promocell, Heidelberg, Germany) were seeded at a density of 5000 cells/ cm^2 and incubated in Osteoblast Growing Medium (Promocell) supplemented to a final concentration of 0.1 ml/ml of foetal calf serum (Promocell) at 37 ° and 5% CO_2 on test surfaces and immunolabelled after 24, 48 h and 7 days. Growth medium was changed every three days. HOB cells did not exceed ten population doublings. Test surfaces were exposed to U.V. light for 20 min. each side, in a laminar flow chamber under sterile conditions, in order to achieve optimal sterilization, prior to cell seeding. The test groups were as follows: PLGA, TiO_2/PLGA-10, TiO_2/PLGA-3, TiO_2/PLGA-100. At least five samples of each type were seeded and analysed in each experiment.

3.4. Cell Morphology and Spreading

Cells were daily examined with the phase contrast microscope in order to evaluate cell morphology, alignment and initial adhesion phase to surfaces. Phenotypic changes, cell distribution and spreading were assessed under light microscopy after staining with toluidine blue, prior to fluorescence and CLSM examination of the PLGA, TiO_2/PLGA-10, TiO_2/PLGA-3, TiO_2/PLGA-100 samples.

3.5. Actin Cytoskeletal Organization and Vinculin Expression

At the end of each experiment, cells were washed with prewarmed phosphate buffered saline (PBS), pH 7.4, and fixed with 3.7% paraformaldehyde at room temperature, washed, and then permeabilized with 0.1% Triton x-100 (Sigma, St Louis, MI, USA). After washing, cells were preincubated with 1% bovine serum albumin (Sigma) in PBS for 20 min prior to cell immunolabelling for actin cytoskeleton with rhodamine phalloidin (Sigma) and monoclonal anti-vinculin FITC conjugate (Sigma). After 20 min. TiO_2/PLGA-10, TiO_2/PLGA-3, TiO_2/PLGA-100 samples were rinsed with prewarmed PBS prior to mounting with Vectashield ® (Vector, Burlingame, CA, USA).

3.6. Confocal Examination

Samples were visualized using a Leica TCS-SL confocal microscope. At least five samples were analysed for each group to assess surface influence on cytoskeletal organization, focal adhesion number, and development and cell morphology. Images were collected and processed using Leica imaging software. At least 50 cells per sample were analyzed. Samples were exposed to the lowest laser power that was able to produce a fluorescent signal for a time interval not higher than 5 min to avoid photobleaching. A pinhole of 1 Airy unit was used. Images were acquired at a resolution of 512 × 512, mean voxel size of 209.20 nm.

3.7. Statistical Analysis

A descriptive analysis was used to summarize the number of contacts in each experimental group. Thereafter for the variable "number of contacts", clearly not normal, the nonparametric contrast Kruskal-Wallis (K-W), first, and later the contrast of two-way ANOVA with the ranges of this variable were used [20]. Finally, the Student-Newman-Keuls (S-N-K) contrast *post hoc* was carried out to detect the differences among the experimental groups.

4. Conclusions

To maintain proper functionality, cells rely on adhesions to and interactions with the surrounding substrate, structure or extracellular matrix. The surrounding microenvironment provides a construct in which cells move, orient, organize and differentiate to form cultures and tissues. Precise definition of three-dimensional microstructural information will allow the development of mechanical models that predict states of stress and strains based on cell-scaffold biomechanics.

This study demonstrated that even an advanced membrane surface with nanofeature can be further enhanced for its bone-integration capability using the novel PECVD functionalization methodology described. Because this plasma modification process is independent from the material underlying, and is fully compatible with polymeric substrates, this methodology has resulted quite appropriate for the controlled functionalization of PLGA substrates to enhance their bioactivity towards the growth of osteoblast cells. In the course of this investigation we have also shown that PLGA substrates partially covered with TiO_2 patches present a clear bioactivity, which is enhanced when the polymer is completely covered with a continuous layer of TiO_2. The different chemical and wetting properties of the activated TiO_2 surface, with regard to those of PLGA rather than a different topography have been claimed as the main factor contributing to the cell growth. This situation has been ascertained by applying the Tougaard background substration method to the XPS spectra, a novel methodological approach that, to our knowledge, has not previously used with oxide/polymer systems. The results presented herein may contribute to a better understanding of the processes involved in the GTR.

Acknowledgments

We thank Junta de Andaluc á (P09CTS5189), Spanish Ministry for Science and Innovation (Instituto de Salud Carlos III (FIS PI 0900508) (CONSOLIDER CSD2008-00023 and MAT2010-21228) for financial support. Patent P201232018 pending.

Author Contributions

Mercedes Salido and Jose Vilches designed the *in vitro* experimental research, performed the cell culture and immunolabelling protocols and the light and confocal microscopic examination and are responsible for the integration of data and the writing of the final version of the paper. Jose Vilches is head of the Research Group Pathobiology in the University of Cadiz. Salido is the main researcher of PI 09/00508, which partially granted the research. Jose I Vilches performed the odontological background, and advised in the osteoblasts culture. Emilio de la Orden, as technician and PhD student, contributed with cell culture and performed the image analysis in collaboration with Antonia Terriza,

and also both contributed in data processing for the statistical procedure, performed by Juan L. Gonzalez-Caballero. Terriza executed the synthesis and characterization by XPS of the TiO_2/PLGA, analysing furthermore their wetting behavior. The deposition of the TiO_2 nanostructures on the PLGA membranes was carried out by Terriza and Ángel Barranco. Francisco Yubero performed the background analysis of XPS spectra to deduce the degree of coverage by the oxide of the polymer membrane. Agustín R. González-Elipe contributed with the general disscussion of the results and executed the design and critical evaluation of experimentas and different working conditions to prepare and characterize the TiO_2/PLGA membranes before the cell adhesion studies. Barranco, Yubero and González-Elipe are both reasearcher of the Nanotechnology of Surfaces Research Group from Instituto de Ciencia de Materiales de Sevilla.

Conflicts of Interest

The authors declare no conflict of interest.

References

1. Chen, G.; Xia, Y.; Lu, X.; Zhou, X.; Zhang, F.; Gu, N. Effects of surface functionalization of PLGA membranes for guided bone regeneration on proliferation and behavior of osteoblasts. *J. Biomed. Mater. Res. A* **2013**, *101*, 44–53.
2. Ikeda T, Hagiwara Y, Hirota M, Tabuchi M, Yamada M, Sugita Y, Ogawa T. Effect of photofunctionalization on fluoride-treated nanofeatured titanium. *J. Biomater. Appl.* **2013**, *2013*, doi:10.1177/0885328213501566.
3. Intranuovo, F.; Favia, P.; Sardella, E.; Ingrosso, C.; Nardulli, M.; d'Agostino, R.; Gristina, R. Osteoblast-like cell behavior on plasma deposited micro/nanopatterned coatings. *Biomacromolecules* **2011**, *12*, 380–387.
4. Bernstein, A.; Tecklenburg, K.; Südkamp, P.; Mayr, H.O. Adhesion and proliferation of human osteoblast-like cells on different biodegradable implant materials used for graft fixation in ACL-reconstruction. *Arch Orthop. Trauma Surg.* **2012**, *132*, 1637–1645.
5. Oliveira D.P.; Palmieri, A.; Carinci, F.; Bolfarini, C. Osteoblasts behavior on chemically treated commercially pure titanium surfaces. *J. Biomed. Mater. Res. A* **2013**, *2013*, doi:10.1002/jbm.a.34855.
6. Gulati, K.; Ramakrishnan, S.; Aw, M.S.; Atkins, G.J.; Findlay, D.M.; Losic, D. Biocompatible polymer coating of titania nanotube arrays for improved drug elution and osteoblast adhesion. *Acta Biomater.* **2012**, *8*, 449–456.
7. Bettinger C.J.; Langer, R.; Borenstein, J.T. Engineering substrate topography at the micro and nanoscale to control cell function. *Angew Chem. Int. Ed.* **2009**, *48*, 5406–5415.
8. Terriza, A.; Díaz-Cuenca, A.; Yubero, F.; Barranco, A.; González-Elipe, A.R.; González-Caballero, J.L.; Vilches, J.; Salido, M. Light induced hydrophilicity and osteoblast adhesion promotion on amorphous TiO_2. *J. Biomed. Mater. Res. A* **2013**, *101*, 1026–1035.
9. Pearce, A.I.; Pearce, S.G.; Schwieger, K.; Milz, S.; Schneider, E.; Archer, C.W.; Richards, R.G. Effect of surface topography on removal of cortical bone screws in a novel sheep model. *J. Orthop. Res.* **2008**, *26*, 1377–1383.

10. Hayes, J.S.; Vos, D.I.; Hahn, J.; Pearce, S.G.; Richards, R.G. An *in vivo* evaluation of surface polishing of TAN intermedullary nails for ease of removal. *Eur. Cells Mater.* **2009**, *18*, 15–26.
11. Isaac, J.; Galtayries, A.; Kizuki, T.; Kokubo, T.; Berdal, A.; Sautier, J.M.; Bioengineered titanium surfaces affect the gene-expression and phenotypic response of osteoprogenitor cells derived from mouse calvarial bones. *Eur. Cells Mater.* **2010**, *20*, 178–196.
12. Yang, J.; Wang, J.; Yuan, T.; Zhu, X.D.; Xiang, Z.; Fan, Y.J.; Zhang, X.D. The enhanced effect of surface microstructured porous titanium on adhesion and osteoblastic differentiation of mesenchymal stem cells. *J. Mater. Sci. Mater. Med.* **2013**, *24*, 2235–2246.
13. Pathak, A.; Deshpande, V.S.; Mc Meeking, R.M.; Evans, A.G. The simulation of stress fibers and focal adhesion development in cells on patterned substrates. *J. R Soc. Interface* **2008**, 5, 507–524.
14. Salido, M.; Vilches, J.I.; Gutiérrez, J.L.; Vilches, J. Actin cytoskeletal organization in human osteoblasts grown on different dental titanium implant surfaces. *Histol. Histopathol.* **2007**, *22*, 1355–1364.
15. Geiger, B.; Spatz, J.P.; Bershadsky, A.D. Environmental sensing through focal adhesions. *Nat. Rev. Mol. Cell. Biol.* **2009**, *10*, 21–33.
16. Coyer, S.R.; Singh, A.; Dumbauld, D.W.; Calderwood, D.A.; Craig, S.W.; Delamarche, E.; García, A.J. Nanopatterning reveals an ECM area threshold for focal adhesion assembly and force transmission that is regulated by integrin activation and cytoskeleton tension. *J. Cell. Sci.* **2012**, *125*, 5110–5123.
17. Borrás, A.; Cotrino, J.; González-Elipe, A.R. Type of plasmas and microstructures of TiO_2 thin films prepared by plasma enhanced chemical vapor deposition. *J. Electrochem. Soc.* **2007**, *154*, 152–157.
18. López-Santos, M.C.; Yubero, F.; Espinós, J.P.; González-Elipe, A.R. Non-destructive depth compositional profiles by XPS peak-shape analysis. *Anal. Bional. Chem.* **2010**, *396*, 2757–2768.
19. Tougard, QUASES, Software Package for Quantitative XPS/AES of Surface Nanostructures by Inelastic Peak Shape Analysis. Available online: http://www.quases.com (accessed on 28 February 2014).
20. Shah, D.A.; Madden, L.V. Nonparametric analysis of ordinal data in designed factorial experiments. *Phytopathology* **2004**, *94*, 33–43.
21. Smith, L.J.; Swaim, J.S.; Yao, C.; Haberstroh, K.M.; Nauman, E.A.; Webster, T.J. Increased osteoblast cell density on nanostructured PLGA-coated nanostructured titanium for orthopedic applications. *Int. J. Nanomed.* **2007**, *2*, 493–499.
22. Balasundaram, G.; Webster, T.J. An overview of nano-polymers for orthopedic applications. *Macromol. Biosci.* **2007**, *7*, 635–642.
23. Webster, T.J.; Miller, D.C.; Thapa, A.; Haberstroh, K.M. *In vitro* Vascular Cell Adhesion and Proliferation on Alkaline Degraded Poly-Lactic/Glycolic Acid Polymers. In *Biological Biomimetic Materials: Properties to Function*; Aizenberg, J., McKittrick, J.M., Orme, C.A., Eds.; Materials Research Society: Warrendale, PA, USA, 2002; pp. 51–56.
24. Salido, M, Vilches, J.I.; Gonzalez, J.L.; Vilches, J. Implant surface microtopography induces mitochondrial bioenergetics and distribution in living human osteoblasts. *Histol. Histopathol.* **2009**, *24*, 1275–1286.

25. Vilches, J.; Vilches-Perez, J.I; Salido, M. Cell-Surface Interaction in Biomedical Implants Assessed by Simultaneous Fluorescence and Reflection Confocal Microscopy. In *Modern Research and Educational Topics in Microscopy*; Vilas, M., Ed.; Formatex: Badajoz, Spain, 2007; pp. 60–67.
26. Salido, M.; Vilches, J.I.; Vilches J. Simultaneous Fluorescence and Reflection Confocal Microscopy Study of Living Osteoblast Bioenergetics as a Tool for the Design of Surface Topography of Dental Implants. In *Dental Material Research*; Kaminski, H.D., DuPois, E.A., Eds.; Nova Science Publishers: New York, NY, USA, 2009; pp. 61–82.
27. Barranco, A.; Cotrino, J.; Yubero, F.; Espinós, J.P.; Benítez, J.; Clerc, C.; González-Elipe, A.R. Synthesis of SiO_2 and $SiO_xC_yH_z$ thin films by microwave plasma CVD. *Thin Solids Films* **2001**, 401, 150–158.
28. Tougard, S. Surface nanostructure determination by x-ray photoemission spectroscopy peak shape analysis. *J. Vac. Sci. Technol.* **1996**, *14*, 1415–1423.
29. Diener, A.; Nebe, B.; Luthen, F.; Becker, P.; Beck, U.; Neumann, H.G.; Rychly J. Control of focal adhesion dynamics by material surface characteristics. *Biomaterials* **2005**, *26*, 383–392.
30. Rape, A.D.; Guo, W.; Wang, Y. The regulation of traction force in relation to cell shape and focal adhesions. *Biomaterials* **2011**, *32*, 2043–2051.
31. Chen, C.S.; Alonso, J.L.; Ostuni, E.; Whitesides, G.M.; Ingber D.E. Cell shape provides global control of focal adhesion assembly. *Biochem. Biophys. Res. Commun.* **2003**, *307*, 355–361.
32. Hu, K.; Ji, L.; Applegate, K.T.; Danuser, G.; Waterman-Storer, C.M. Differential transmission of actin motion within focal adhesions. *Science* **2007**, *315*, 111–115.
33. Zimerman, B.; Arnold, M.; Ulmer, J.; Blümmel, J.; Besser, A.; Spatz, J.P.; Geiger, B. Formation of focal adhesion-stress fiber complexes coordinated by adhesive and non-adhesive surface domains. *IEEE Proc. Nanobiotech.* **2004**, *151*, 62–66.
34. McNamara, L.E.; Sjöström, T.; Burgess, K.E.V.; Kim, J.J.W.; Liu, E.; Gordonov, S.; Moghe, P.V.; Meek, R.M.; Oreffo, R.O.; Su, B.; *et al.* Skeletal stem cell physiology on functionally distinct titania nanotopographies. *Biomaterials* **2011**, *32*, 7403–7410.
35. Lamers, E.; te Riet, J.; Domanski, M.; Luttge, R.; Figdor, C.G.; Gardeniers, J.G.; Walboomers, X.F.; Jansen, J.A. Dynamic cell adhesion and migration on nanoscale grooved substrates. *Eur. Cells Mater.* **2012**, *23*, 182–193.
36. Humphries, J.D.; Wang, P.; Streuli, C.; Geiger, B.; Humphries, M.J.; Ballestrem, C. Vinculin controls focal adhesion formation by direct interactions with talin and actin. *J. Cell Biol.* **2007**, *179*, 1043–1057.
37. Wolfenson, H.; Bershadsky, A.; Henis, Y.I.; Geiger, B. Actomyosin-generated tension controls the molecular kinetics of focal adhesions. *J. Cell Sci.* **2011**, *124*, 1425–1432.
38. Miyauchi, T.; Yamada, M.; Yamamoto, A.; Iwasa, F.; Suzawa, T.; Kamijo, R.; Baba, K.; Ogawa, T. The enhanced characteristics of osteoblast adhesion to photofunctionalized nanoscale TiO_2 layers on biomaterials surfaces. *Biomaterials* **2010**, *31*, 3827–3839.
39. Biggs, M.J.; Richards, R.G.; Dalby, M.J. Nanotopographical modification: a regulator of cellular function through focal adhesions. *Nanomedicine* **2010**, *6*, 619–633.
40. Tougard, S. Accuracy of the non-destructive surface nanostructure quantification technique based on analysis of the XPS or AES peak shape. *Surf. Interface Anal.* **1998**, *26*, 249–269.

41. Espinós, J.P.; Martín-Concepción, A.I.; Mansilla, C.; Yubero, F.; González-Elipe, A.R. X-ray photoelectron spectroscopy study of the nucleation processes and chemistry of CdS thin films deposited by sublimation on different solar cell substrate materials. *J. Vac. Sci. Technol.* **2006**, *24*, 919–928.
42. Mansilla, C.; Gracia, F.; Martin-Concepción, A.I.; Espinós, J.P.; Holgado, J.P.; Yubero, F.; González-Elipe, A.R. Study of the first nucleation steps of thin films by XPS inelastic peak shape analysis. *Surface. Interface Anal.* **2007,** *39*, 331–336.
43. López Santos, C.; Yubero, F.; Cotrino, J.; Barranco, A.; González-Elipe, A.R. Plasmas and atom beam activation of the surface of polymers. *J. Phys. D Appl. Phys.* **2008**, *41*, 225209–225221.